From the interface energy to the solubility limit of aluminium in nickel from first-principles and Kinetic Monte Carlo calculations

Céline Hin, Joël Lépinoux, Jeffrey Neaton, Mildred Dresselhaus

From the interface energy to the solubility limit of aluminium in nickel from first-principles and Kinetic Monte Carlo calculations

Céline Hin [a,*], Joël Lépinoux [b], Jeffrey B. Neaton [c], Mildred Dresselhaus [d]

a Department of Mechanical Engineering, Massachusetts Institute of Technology, Cambridge, MA 02139-4307, USA
b SIMaP, Grenoble INP, UJF, CNRS, 38402 Saint Martin D'Heres, France
c Molecular Foundry, Lawrence Berkeley National Laboratory, University of California, Berkeley, CA 94720-1730, USA d Department of Physics, Massachusetts Institute of Technology, Cambridge, MA 02139-4307, USA

We developed a way to predict the solubility limit of solute atoms in a binary alloy using a Kinetic Monte Carlo algorithm. The idea is to use the interface energies calculated by first-principles calculations to parameterize the pair interaction energies used in the Kinetic Monte Carlo algorithm. In order to validate this method, it was tested on a very well known case: the Ni-Al alloy. We found that the calculations are in very good agreement with the previously calculated phase diagrams.

1. Introduction

In the last two decades, considerable efforts have been devoted to develop methods for calculating composition-temperature phase diagrams from first principles calculations. These methods have been developed as an alternative to laboratory experimentation, where phase diagrams could be very difficult to determine, especially for multi-component systems. The first few studies were devoted to only consider substitutional effects, which were good enough to reproduce the topology of most phase diagrams. However, better accuracies with experimental data have now been achieved which take into the account of electronic excitations [1] as well as lattice vibrations [2–4]. Such excitations could play important roles in determining the relative stability of the different relevant phases.

In this study, we developed a method to predict the solubility limit of solute atoms in a binary alloy using a kinetic Monte Carlo (KMC) approach. The idea is to use the interface energies calculated by first-principles calculations to parameterize pair interaction energies used in a KMC algorithm.

In order to validate this method, it was tested on a very well known case: the Ni–Al alloy. The richest Ni intermediate phase in the Ni–Al phase diagram is Ni_3Al. This compound has an $L1_2$ structure with four atoms per unit cell [5]. The solubility limit of Al in Ni is very high, the maximum solubility being 21 at.% at about 1643 K. Kaufman and Nesor [6] were the first to calculate the phase diagram of the Al–Ni system. They considered the B2 phase to be disordered with a body-centered cubic-A2 structure. The phases Ni_3Al, AlNi, and Al_3Ni were all assumed to be stoichiometric. The cluster variation method developed by Kikuchi et al. [7,8] has also been extensively used [9–13] to calculate a part of or the entire phase diagram for non-stoichiometric phases. Du and Clavaguera [14] calculated the Al–Ni phase diagram, but did not consider the ordering in the face-centered cubic (FCC) phase, and they used the associated model to describe the thermodynamic properties of the liquid phase [15–17]. More recently, different phase diagrams have been calculated combining calorimetry, and *Calphad*, which stands for a calculation of phase diagrams [18,19]. Only one experimental phase diagram has been reported experimentally for Ni–Al [20]. The comparison with our calculated solubility limit is chosen to be based on the data in Ref. [18].

In the next section, we present the thermodynamic and the kinetic set of parameters used here to determine the phase diagram. The thermodynamic parameters have been determined by first-principles calculations. The cohesive energies of each single phase (e.g. the Ni and Al FCC phase), and the enthalpy of formation of the Ni_3Al precipitate have been calculated, as well as the [1 0 0] interface energy between the Ni matrix and the Ni_3Al precipitate. The kinetic parameters have been fit to reproduce the experimental results of self and impurity diffusion coefficients. Solubility limits obtained from the KMC method are presented. Finally, the geometrical shape of the Ni_3Al precipitate is determined by KMC

* Corresponding author. Tel.: +1 617 253 7413; fax: +1 617 324 5519.
E-mail address: celine_hin@yahoo.fr (C. Hin).

Table 1
Cohesive energies (eV/at.%) obtained by first-principles calculations and compared with experimental data [29,30].

FCC phase	Cohesive energies (eV/at.%)	
	DFT (GGA)	Experiment
Ni	4.32	4.44 [29]
Al	3.62	3.43 [30]

simulations and is compared with the Wulff Shape [21] calculated with the Wullfman program [22]. The comparison demonstrates good agreement between both precipitate shapes. The accurate shape as well as the correct solubility limit obtained by the KMC algorithm emphasizes on the idea that the interface energies could contain the thermodynamic information that is needed to describe a physical system.

2. Parameterization

Thermodynamic parameters depend on order energies $\omega^{(n)} = \varepsilon^{(n)}_{\mathrm{NiAl}} - (1/2)\varepsilon^{(n)}_{\mathrm{NiNi}} - (1/2)\varepsilon^{(n)}_{\mathrm{AlAl}}$, where $\varepsilon^{(n)}_{XY}$ are the pair interaction energies between two atoms, which include the nth nearest-neighbor interaction energies. In this study, order energies up to $n = 2$ are considered to be sufficient to adequately reproduce the thermodynamics of the system.

All the free energy calculations are performed using first-principles density functional theory. They have been carried out using the *ab initio* total-energy and the molecular-dynamics program VASP (Vienna *ab initio* simulation package) [23,24] employing ultrasoft pseudopotentials [25] and an expansion of the electronic wave functions in plane waves with a kinetic-energy cutoff of 281 eV. All calculated results were derived employing the generalized gradient approximation (GGA) due to Perdew and Wang [26]. Brillouin-zone integrations were performed using Monkhorst and Pack [27] k-point meshes, and the Methfessel and Paxton [28] technique with a 0.1 eV smearing of the electronic levels. The simulations used 400 k-points in the irreducible Brillouin zone meshes to ensure the absolute convergence of the total energy to within a precision of better than 2.5 meV/atom. Spin polarization was used since nickel is magnetic.

The first nearest neighbor pair interaction energies $\varepsilon^{(1)}_{\mathrm{NiNi}}$ and $\varepsilon^{(1)}_{\mathrm{AlAl}}$ were derived from cohesive energies (which is the difference between the energy per atom of a system of free atoms at rest far apart from each other, and the energy of the solid) of the nickel and the aluminium FCC structures according to:

$$E_{\mathrm{coh}}(X) = \frac{z_1}{2}\varepsilon^{(1)}_{XX} \tag{1}$$

where z_1 is the number of atoms in first neighbor positions. The first nearest neighbor pair interaction energy $\varepsilon^{(1)}_{\mathrm{NiAl}}$ was determined from these first nearest neighbor pair interaction energies $\varepsilon^{(1)}_{\mathrm{NiNi}}$ and $\varepsilon^{(1)}_{\mathrm{AlAl}}$, and the relation $\Delta E(\mathrm{Ni_3Al}) = 3\omega^{(1)}$, which is the enthalpy of formation of the Ni_3Al intermetallic phase (i.e., the change of enthalpy that accompanies the formation of 1 mol of a substance in its standard state from its constituent elements in their standard states). The results of the cohesive energies and of the enthalpy of formation of Ni_3Al precipitate are listed in Tables 1 and 2. We note that for all these values, there is very good agreement between the calculated values and the experimental data [29–31]. The calculated values for $\varepsilon^{(1)}_{XY}$ are given in Table 3.

In order to determine the second nearest neighbor pair interaction energies, it is needed to find out the order energy $\omega^{(2)}$ (i.e. the difference between the ⟨1 1 0⟩ bond energy of a Ni–Al pair of atoms and half sum of the ⟨1 1 0⟩ bond energies of Ni–Ni and Al–Al pairs of atoms), which can be expressed in terms of the interface

Table 2
Enthalpy of formation (eV/at.%) obtained by first-principles calculations and compared with experimental data [31].

Phase	Free enthalpy of formation (eV/at.%)	
	DFT (GGA)	Experiment
Ni (FCC)	0.	0.
Al (FCC)	0.	0.
Ni_3Al ($L1_2$)	−0.44	−0.41 [31]

Table 3
Pair interaction energies (in eV) of the NiAl system on a FCC lattice.

X–Y interactions	$\varepsilon^{(1)}_{XY}$ (eV)	$\varepsilon^{(2)}_{XY}$ (eV)
Ni–Ni	−0.72	0
Al–Al	−0.60	0
Ni–Al	−0.80	0.0317
Ni–V	−0.2208	0
Al–V	−0.2227	0
V–V	−0.2000	0.3200

energy through Eq. (2) for the specific case of Ni_3Al precipitate in the Ni matrix. The interface energies between the solid solution is supposed to be in equilibrium and the $L1_2$ precipitates calculated for the [1 0 0] direction of the interface. If the structures Ni/Ni_3Al are stoichiometric, a simple broken bond calculation [32–34] leads to:

$$\omega^{(2)} = a^2\sigma_{1\,0\,0} \tag{2}$$

where a is the lattice constant of Ni, and $\sigma_{1\,0\,0}$ is the interface energy for the [1 0 0] interface. $\omega^{(2)}$ is given by:

$$\omega^{(2)} = \varepsilon^{(2)}_{\mathrm{NiAl}} - \frac{1}{2}\varepsilon^{(2)}_{\mathrm{NiNi}} - \frac{1}{2}\varepsilon^{(2)}_{\mathrm{AlAl}} \tag{3}$$

where $\varepsilon^{(2)}_{XY}$ are the pair interaction energies between two atoms (X and Y), which include the second nearest-neighbor interaction energy.

In Eq. (2), it is necessary to consider for the [1 0 0] direction a periodic system having two interfaces as shown in Fig. 1, where the $L1_2$ structure consists of an alternation of a pure Ni plane and a mixed plane containing Ni and Al atoms. In this configuration, we have to determine the reference state for the Ni plane located at the interface. Since the $L1_2$ structure is stoichiometric, one of these planes belongs to the compound Ni_3Al and the second plane belongs to the pure FCC Ni phase.

Interface energy calculations have been performed in the present work using first-principles methodologies. From these calculations, the [1 0 0] interface energy between the $L1_2$ structure and the FCC Ni phase is found to be equal to 41 mJ m^{-2}. The [1 0 0] interface energy is in good agreement with data found in the literature, which give a wide range of energies between 0.9 and 90 mJ m^{-2}

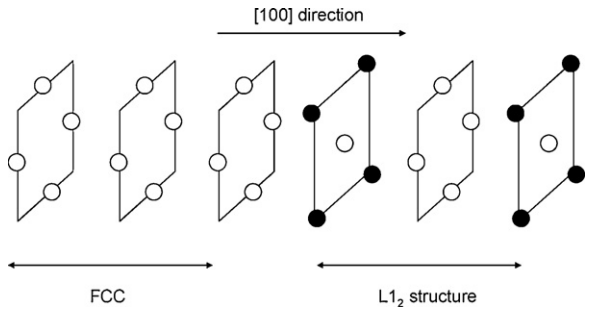

Fig. 1. The periodic system used to calculate the interface energy between the $L1_2$ structure Ni_3Al and the FCC nickel phase in the [1 0 0] direction. White spheres are Ni atoms and black spheres are Al atoms.

Table 4
Attempt frequencies (in s^{-1}) and saddle-point binding energies of X atoms (in eV).

	Ni	Al
ν_X^0 (s^{-1})	1.1×10^{16}	1.1×10^{16}
e_X^{SP} (eV) (in the bulk)	−9.75	−9.22

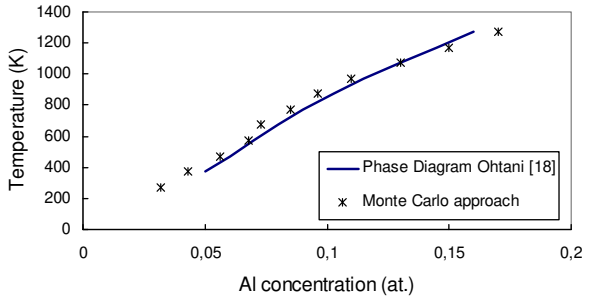

Fig. 2. Solubility limits of aluminium in nickel determined from first principles calculations coupled with a mean field approximation or a kinetic Monte Carlo method and compared to the data of Ohtani et al. [18].

[35–38]. If we assume that $\varepsilon^{(2)}_{\mathrm{NiNi}} = \varepsilon^{(2)}_{\mathrm{AlAl}} = 0\,\mathrm{eV}$, one then obtains $\varepsilon^{(2)}_{\mathrm{NiAl}} = 0.0317\,\mathrm{eV}$ from our calculations. This value is very close to the estimation given by Abinandanan obtained from the phase diagram [39], which gives a value of 0.032 eV.

With the calculated set of parameters, the ratio $(\omega^{(1)}/\omega^{(2)}) < 0$ was found, with $\omega^{(1)} = -0.146\,\mathrm{eV}$ and $\omega^{(2)} = 0.037\,\mathrm{eV}$. This ensures the formation of an ordered structure Ni_3Al.

The pair interaction energies between atoms and vacancies in first neighbor positions, and between two vacancies have also been determined by first-principles calculations. They are here recalled in Table 3.

3. Kinetic Monte Carlo simulations

We use a KMC simulation method developed in Ref. [42], which is based on the description of the atomic diffusion mechanisms that control precipitation. Thus, in addition to the thermodynamic parameters determined in Section 2, we also need kinetic parameters, which include the saddle-point binding energies, and the attempt frequencies. They have been determined in Refs. [42,44], and are recalled here in Table 4. This set of parameters has been used to estimate the solubility limit of Ni_3Al in nickel and the equilibrium shape of the precipitates.

3.1. Solubility limit calculations

The simulation boxes used in our calculations consist of $200 \times 200 \times 200$ FCC unit cells with full periodic boundary conditions. The solubility limit has been estimated using a canonical ensemble. In a simulation box, a large precipitate of Ni_3Al has been embedded in the nickel matrix. To avoid Gibbs–Thomson effects, the precipitate has planar interfaces. Through the mechanism of diffusion by a vacancy jump [42] between the two phases Ni and Ni_3Al at constant temperature, we determine the concentration in aluminium within the nickel phase at equilibrium. In order to make a good estimation of the concentration of aluminium in the solid solution for a biphasic precipitate/matrix equilibrium situation, the model system calculation has to explore enough configurations (e.g. 10^5 steps). This method thus gives a good approximation for the solubility limit of the precipitated phase at a temperature T in the host material.

As seen in Fig. 2, the agreement between the calculation of Ohtani et al. [18] and our KMC calculation is quite accurate over the temperature range 300–1300 K. Even though the parameters come from the calculation of the interface energy calculated at 0 K, the KMC results give very satisfactory quantitative agreement with previous calculations since the KMC is a method that naturally takes into account the entropic effects linked to the temperature.

Thus, in the KMC calculations, the thermodynamic information (namely the ordered structure and the solubility limit) is contained within the pair interaction energies determined from the interface energy. It is an easy task calculating the interface energies by first-principles calculations since the ground state of each phase is well-known. Another way to calculate the pair interaction energies could be to estimate them directly from first-principles calculations without determining the interface energies. However, there are a large amount of configurations in such systems, which make irrelevant the choice of the configuration which will accurately reproduce the thermodynamic information.

Finally, from a similar calculation detailed in Ref. [40] and based on the Bragg–Williams approximation [41], the solubility limit c^{eq} of an A_3B phase only depends on the second nearest-neighbor order energy $\omega^{(2)}$:

$$c^{\mathrm{eq}} = \exp\left(-\frac{6 \times \omega^{(2)}}{kT}\right) \tag{4}$$

where k is the Boltzmann constant and T is the temperature. The Bragg–Williams approximation is a mean field approximation. It only considers the interactions between different sites of the lattice through their average occupancies and neglects all correlation effects between these occupancies. Consequently, there is no short range ordering effect introduced into this model in the homogeneous phase and it is not possible to quantify the influence of $\omega^{(1)}$ on the solubility limit. However, the KMC simulations developed in Ref. [42], which are based on a description of the atomic diffusion mechanisms that control precipitation, do not make such assumptions. For example, a change of 10% in $\omega^{(1)}$ gives a change of 0.23% (in absolute value) on the solubility limit calculated by the KMC method at 600 K. This is mainly due to the anti-site defect concentration, which may vary as a function of $\omega^{(1)}$. Thus, a change of $\omega^{(1)}$ only induces a slight change on the solubility limit. Despite its weak influence on the solubility limit, it is important to have a good approximation of $\omega^{(1)}$, in particular for concentrated alloys. Indeed, neglecting this point, for instance taking $\omega^{(1)}$ infinite (in absolute value), the only possible choice in mesoscopic models like Cluster Dynamics [43], systematically leads to a solubility limit smaller than the values obtained with a correct approximation for $\omega^{(1)}$. For solubility limits in the range 5–10 at.%, the shift can be of the order of 1 at.%.

To conclude, the complete parameterization of the KMC model as done here can be simplified as long as only thermodynamic properties are concerned, e.g. the solubility limit. Indeed, in the present case it is widely accepted that thermodynamics properties depend only on $\omega^{(2)}$ in first order and on $\omega^{(1)}$ or alternatively on $\omega^{(1)}/\omega^{(2)}$ in second order. This feature allows for a rapid evaluation of KMC input data when its use is restricted to the exploration of thermodynamic properties as performed in Ref. [43].

3.2. Shape of the precipitates

To emphasize the idea that the interface energies could contain enough thermodynamic information that is needed to describe a physical system, the equilibrium shape of the precipitates has been investigated by KMC simulations at 400 K and the result thus obtained was compared with the Wulff construction [21] implemented in the Wulffman program [22]. In the Wulff model, the equilibrium crystal shape of a particle of a given volume embedded within another homogeneous phase results from a geometric

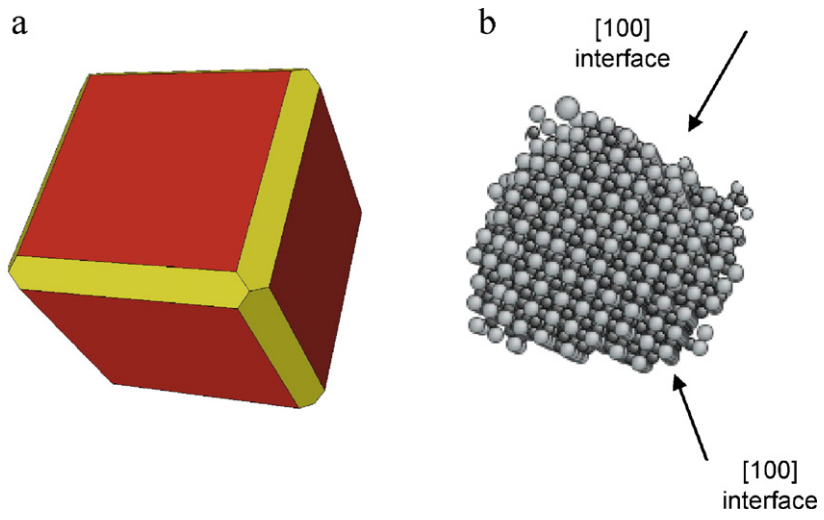

Fig. 3. (a) Wulff construction [21] of the shape of a Ni_3Al precipitate in a nickel matrix determined from the Wulffman program [22]. Interface energies are: $\sigma_{100} = 41\,mJ\,m^{-2}$, $\sigma_{110} = 58\,mJ\,m^{-2}$, $\sigma_{111} = 71\,mJ\,m^{-2}$. (b) Shape of a Ni_3Al precipitate in a nickel matrix obtained by Monte Carlo calculations at 400 K with the set of parameters given in Table 3. Ni atoms are in black and Al atoms are in grey.

construction that is derived from minimizing the total interfacial energy of a particle of fixed volume through the integral $\int \sigma(\hat{n})dA$, where $\sigma(\hat{n})$ describes the interface energy as a function of the surface normal $\hat{n}$ [21]. Thus, this model requires the calculation of many interface energies in different directions.

In the present study, we have determined two additional free interface energies to calculate the Wulff construction. Specifically, from the [1 0 0] interface energy, we have determined the interface energies for the [1 1 0] and [1 1 1] directions. If the structures Ni/Ni_3Al are stochiometric, the broken bond model [32–34] gives the following relations:

$$\sigma_{100} = \frac{1}{\sqrt{2}}\sigma_{110} = \frac{1}{\sqrt{3}}\sigma_{111} \tag{5}$$

where σ_{110}, and σ_{111} are the interface energies in the [1 1 0] direction, and the [111] direction, respectively. The interface energies [1 0 0], [1 1 0], and [1 1 1] are thus found to be equal to 41, 58, 71 mJ m^{-2}, respectively.

Introducing the interface energies calculated from Eq. (5) into the Wulffman program [22] based on the Wulff construction [21], we have obtained the shape of the precipitate as shown in Fig. 3a. Only the two lowest interface energies [1 1 0] and [1 0 0] are observed in our calculations. The orientated face [1 1 1], having an interface energy considerably greater than the other two, disappears when calculating the minimum energy shape. The shape obtained for a Ni_3Al precipitate in the bulk of the material is thus the polyhedron containing the [1 1 0] and [1 0 0] interface orientations as represented in Fig. 3a. The Ni_3Al precipitate, determined by the KMC simulation, thus adopts a morphology very close to that predicted by the Wulff construction, i.e. the cluster shape is basically a cube dominated by large [1 0 0] faces while edges tend to exhibit [1 1 0] facets (Fig. 3b). Comparisons of the calculated shape with experimental shapes give satisfactory agreement [45].

4. Conclusion

To conclude, in order to determine the solubility limit of aluminium in nickel, we use the interface energy calculated by first-principles calculations to parameterize pair interaction energies used in the Kinetic Monte Carlo algorithm. Thus first-principles calculations combined with a KMC method provide very powerful and easy-to-use tools to calculate the solubility limit. For further study, this method could be extended to calculate solubility limits that are difficult to estimate directly from experiments in multi-component systems and with atoms located in substitutional or/and interstitial positions.

Acknowledgements

We gratefully acknowledge useful and stimulating discussions with Professor W.C. Carter. The authors gratefully acknowledge the financial support of the Department of Energy under Grant DE-FG02-08ER46516.

References

[1] C. Wolverton, A. Zunger, Phys. Rev. B 52 (1995) 8813.
[2] G.D. Garbulsky, G. Ceder, Phys. Rev. B 49 (1994) 6327.
[3] V. Ozolins, M. Asta, Phys. Rev. Lett. 86 (2001) 448.
[4] E. Clouet, J.M. Sanchez, C. Sigli, Phys. Rev. B 65 (2002) 094105.
[5] P.V. Mohan Rao, K. Satyanarayana Murthy, S.V. Suryanarayana, S.V. Nagender Naidu, Phys. Status Solidi A 133 (1992) 231.
[6] I. Kaufman, H. Nesor, Calphad 2 (4) (1978) 325.
[7] R. Kikuchi, Phys. Rev. 81 (6) (1931) 988.
[8] R. Kikuchi, D. de Fontaine, in: C. Carter (Ed.), Proc. Applications of Phase Diagram in Metallurgy and Ceramics, Gaithersburg, USA, January 1977, vol. 2. NBS Special Publication 496, 1978, pp. 967–988.
[9] C. Sigli, J.M. Sanchez, Acta Metall. 33 (1985) 1097.
[10] A.E. Carlsson, J.M. Sanchez, Solid State Commun. 65 (6) (1988) 527.
[11] C. Colinet, P. Hicter, A. Pasturel, Phys. Rev. B 45 (4) (1988) 1571.
[12] M. Sluiter, P.E.A. Turchi, F.J. Pinski, G.M. Stocks, J. Phase Equil. 13 (6) (1992) 605.
[13] A. Pasturel, C. Colinet, A.T. Paxton, M. van Schilfgaarde, J. Phys. Condens. Mater. 4 (4) (1992) 942.
[14] Y. Du, N. Clavaguera, J. Alloys Compd. 237 (1996) 20.
[15] F. Dolezalek, Z. Phys. Chem. 64 (1908) 727.
[16] A.S. Jordan, Metall. Trans. 1 (1970) 239.
[17] F. Sommer, Z. Metallkd. 73 (1982) 72.
[18] H. Ohtani, M. Yamano, M. Hasebe, Calphad: Comput. Coupling Phase Diagrams Thermochem. 28 (2004) 177.
[19] J. Miettinen, Calphad: Comput. Coupling Phase Diagrams Thermochem. 29 (2005) 40.
[20] H. Okamoto, J. Phase Equilib. 14 (1993) 257.
[21] G. Wulff, Z. Krystallogr. Mineralog. 34 (5/6) (1901) 449.
[22] A. Roosen, R. McCormack, W.C. Carter, Wulffman, An Interactive Crystal Shape Constructor, CTCMS-NIST, 2002. Disponible à. http://www.ctcms.nist.gov/wulffman.
[23] G. Kresse, J. Furthmuller, Phys. Rev. B 54 (1996) 11169.
[24] G. Kresse, J. Furthmuller, Comput. Mater. Sci. 6 (1996) 15.
[25] D. Vanderbilt, Phys. Rev. B 41 (1990) 7892.
[26] J.P. Perdew, in: P. Ziesche, H. Eschrig (Eds.), Electronic Structure of Solids, vol. 91, Akademie Verlag, Berlin, 1991, p. 11.
[27] H.J. Monkhorst, J.D. Pack, Phys. Rev. B 13 (1976) 5188.
[28] M. Methfessell, A.T. Paxton, Phys. Rev. B 40 (1989) 3616.
[29] P.H.T. Philipsen, E.J. Baerends, Phys. Rev. B 54 (8) (1996) 5326.
[30] R. Gaudoin, W.M.C. Foulkes, G. Rajagopal, J. Condens. Mat. 14 (38) (2002) 8787.

[31] K. Rzyman, Z. Moser, R.E. Watson, M. Weinert, J. Phase Equilib. 17 (1996) 173.
[32] D. Wolf, J. Appl. Phys. 68 (1990) 3221.
[33] W.R. Tyson, W.A. Miller, Surf. Sci. 62 (1977) 267.
[34] D. Wolf, Surf. Sci. 226 (1990) 389.
[35] A. Ardell, Interface Sci. 3 (1995) 119.
[36] R. Banerjee, J.P. Fain, P.M. Anderson, H.L. Fraser, Scripta Mater. 44 (2001) 2629.
[37] Y. Mishin, Acta Mater. 52 (2004) 1451.
[38] Y. Amouyal, Z. Mao, D.N. Seidman, Appl. Phys. Lett. 93 (2008) 201905.
[39] A. Abinandanan, F. Haider, G. Martin, Acta Mater. 46 (12) (1998) 4243.
[40] C. Hin, B.D. Wirth, J.B. Neaton, Phys. Rev. B 80 (2009) 134118.
[41] F. Ducastelle, Order and Phase Stability in Alloys, North-Holland, Amsterdam, 1991.
[42] C. Hin, J. Phys. D: Appl. Phys. 42 (2009) 225309.
[43] J. Lépinoux, C. Sigli, in: Proceedings of Solid-Solid Phase Transformations in Inorganic Materials, Avignon, France, June 2010.
[44] C. Pareige, F. Soisson, G. Martin, D. Blavette, Acta Mater. 47 (1999) 1889.
[45] Y. Ma, A.J. Ardell, Acta Mater. 55 (13) (2007) 4419.